ered with a thin fluorocarbon film. This wafer acted as a handling substrate for the resist. After spin-coating, the polymer was gently soft-baked at 40 °C to evaporate the solvent. The SU-8 was then structured by UV lithography (λ = 365 nm) and post-exposure-baked at 40 °C to polymerize the exposed material. Three-dimensional microsystems were achieved by adding further SU-8 layers and repeating the resist processing steps. The microdevices were finally developed in propylene glycol methyl ether acetate (PGMEA) to remove the unexposed SU-8. After development, the SU-8 structures were released from the fluorocarbon-coated handling wafer by tweezers. The fluorocarbon film exhibits low free surface energy, which reduced the adhesion between the resist and the wafer and eased the release [17]. Before the experiments for stress tailoring, the polymer structures were hard-baked in an oven at 120 °C for 30 min to remove residual resist solvent, which could affect the processing. Moreover, the polymer surface was cleaned in oxygen plasma.

Received: August 12, 2005
Final version: October 4, 2005
Published online: December 14, 2005

[1] G. Genolet, J. Brugger, M. Despont, U. Drechsler, P. Vettiger, N. F. de Rooij, D. Anselmetti, *Rev. Sci. Instrum.* **1999**, *70*, 2398.
[2] W. Zhou, S. M. Kuebler, K. L. Braun, T. Yu, J. K. Cammack, C. K. Ober, J. W. Perry, S. R. Marder, *Science* **2002**, *296*, 1106.
[3] S. R. Sershen, G. A. Mensing, M. Ng, N. J. Halas, D. J. Beebe, J. L. West, *Adv. Mater.* **2005**, *17*, 1366.
[4] M. Boncheva, G. M. Whitesides, *Adv. Mater.* **2005**, *17*, 553.
[5] M. Hopcroft, T. Kramer, G. Kim, K. Takashima, Y. Higo, D. Moore, J. Brugger, *Fatigue Fract. Eng. Mater. Struct.* **2005**, *28*, 735.
[6] G. Voskerician, M. S. Shive, R. S. Shawgo, H. von Recum, J. M. Anderson, M. J. Cima, R. Langer, *Biomaterials* **2003**, *24*, 1959.
[7] T. Yu, C. K. Ober, S. M. Kuebler, W. Zhou, S. R. Marder, J. W. Perry, *Adv. Mater.* **2003**, *15*, 517.
[8] D. Haefliger, B. P. Cahill, A. Stemmer, *Microelectron. Eng.* **2003**, *67–68*, 473.
[9] D. Haefliger, R. Marie, A. Boisen, in *Tech. Digest Transducers '05 Conf.*, IEEE, Piscataway, NJ **2005**, pp. 1569–1572.
[10] J. Chen, C. Liu, *J. Microelectromech. Syst.* **2003**, *12*, 979.
[11] P. O. Vaccaro, K. Kubota, T. Aida, *Appl. Phys. Lett.* **2001**, *78*, 2852.
[12] H. W. Jeong, S. Hata, A. Shimokohbe, *J. Microelectromech. Syst.* **2003**, *12*, 42.
[13] R. R. A. Syms, E. M. Yeatman, V. M. Bright, G. M. Whitesides, *J. Microelectromech. Syst.* **2003**, *12*, 387.
[14] H. Lorenz, M. Laudon, P. Renaud, *Microelectron. Eng.* **1998**, *41–42*, 371.
[15] M. Madou, *Fundamentals of Microfabrication*, CRC Press, Boca Raton, FL **1997**, pp. 219–231.
[16] D. Haefliger, A. Boisen, in *Tech. Digest IEEE MEMS 2005 Conf.*, IEEE, Piscataway, NJ **2005**, pp. 556–559.
[17] D. Haefliger, M. Nordström, P. A. Rasmussen, A. Boisen, *Microelectron. Eng.* **2005**, *78–79*, 88.

DOI: 10.1002/adma.200401928

Synthesis of Mesoporous Organosilicate Films in Supercritical Carbon Dioxide**

By *Rajaram A. Pai* and *James J. Watkins**

Ordered mesoporous metal oxides have potential applications in catalysis,[1] sensing and detection,[2] low-*k* dielectrics,[3] separation,[4] and numerous other areas. Their utility depends primarily on their framework chemistry and morphology, but in some cases pore-surface composition, periodicity of the pore structure, and long-range order are defining factors. Conventional methods for preparation are based on the cooperative assembly of network-forming precursors and structure-directing organic templates, such as surfactants or block copolymers. These methods include sol–gel processes via spin-coating[5] and dip-coating,[6] and hydrothermal processes at the liquid/air and the solid/liquid interfaces.[7] More recently, hybrid mesoporous materials functionalized with organic groups at the internal pore surfaces[8,9] or containing functional organic groups distributed homogeneously within the framework[10,11] have been prepared. Films of homogeneous composition can be directly obtained by direct co-condensation of the silica precursor, tetraethylorthosilicate (TEOS), and organosilicate precursors containing the desired functional group. Alternatively, post-synthesis functionalization of the internal pore surfaces of mesoporous materials can modify the performance of silicate materials with respect to adsorption, wetting, and catalytic properties.[8,12,13] One potential limitation is that the extent of grafting can be limited by the accessibility and number of surface silanol groups. To date, most reports deal with the synthesis of granular materials by either or both of these methods. Numerous applications, however, require uniform, defect-free films. Here, we focus on the rapid preparation of device-quality films using an alternative approach in supercritical carbon dioxide.

This work significantly extends our recent report of a novel method of synthesis of ordered mesostructured films for use as low-*k* dielectrics by the selective mineralization of preorganized block-copolymer templates in supercritical carbon diox-

[*] Prof J. J. Watkins, R. A. Pai[+]
Department of Chemical Engineering
University of Massachusetts Amherst
Amherst, MA 01003 (USA)
E-mail: watkins@ecs.umass.edu
[+] Present address: Portland Technology Development Group, Intel Corporation, Hillsboro, OR 97124, USA.

[**] Funding from the National Science Foundation (CTS-0304159) in support of this work is gratefully acknowledged. Facilities supported by the NSF MRSEC on Polymers at the University of Massachusetts were used for the characterization of materials described in this paper.

ADVANCED MATERIALS

ide.[14] In our approach, structure development within the template and metal-oxide-network formation occur in two discrete steps, which is distinct from traditional cooperative self-assembly processes that involve simultaneous ordering of the organic template and formation of the inorganic network via precursor condensation. The two-step process offers the potential for exceptional control of the mesoporous film structure at multiple length scales through preorganization and manipulation of the template prior to infusion. Moreover, it is rapid and yields uniform, defect-free films over 8 in. (19.6 cm) Si wafers.

Supercritical CO_2 enables in-situ chemistry within the polymer templates by enhancing the diffusivities of small precursor molecules within the dilated film.[15] Controlled dilation of the polymer templates by CO_2 does not disrupt the microphase-separated structure of the block copolymers.[16] Moreover, the solvating properties of the CO_2 can be used to control the distribution of the precursor between the CO_2 and the polymer template.[17] The favorable transport properties of supercritical CO_2, including low viscosity and zero surface tension, offer additional opportunities for the post-synthesis surface modification of metal oxides, including silylation and other surface modifications of porous materials.[18,19] Unlike reactions in liquid solvents, surface modification in CO_2 does not require a subsequent drying step. Moreover, the absence of surface tension in supercritical solutions prevents the collapse of nanoscale features in device structures and mesoporous films, which is a major disadvantage of liquid-based processes.[20]

We have now carried out the preparation of ordered, hybrid, mesoporous organosilicate films by both direct synthesis and post-synthesis functionalization methods in CO_2. The templates employed include alkyl poly(ethylene oxide) surfactants (Brij, Aldrich) and poly(ethylene oxide) (PEO)–poly(propylene oxide)–poly(ethylene oxide) triblock copolymers (Pluronic, BASF). Films of the organic templates were spin-coated from a solution of the template and *para*-toluenesulfonic acid (*p*TSA) in ethanol. *p*TSA, which serves as the acid catalyst for precursor condensation during the infusion step, partitions selectively into the hydrophilic PEO domains of the template during spin-coating. Confinement of *p*TSA to the PEO domain results in a rapid, highly efficient and selective subsequent mineralization step. Both the as-infused and the calcined films were characterized using conventional θ–θ X-ray diffraction (XRD), Fourier-transform infrared (FTIR) spectroscopy, and transmission electron microscopy (TEM). The calcined films were also characterized using spectroscopic ellipsometry (SE).

Figure 1 shows the XRD patterns of a series of silica and organosilicate films that were prepared using Brij 78 ($C_{18}H_{37}(CH_2CH_2O)_{20}OH$) templates, and mixtures of TEOS and methyltriethoxysilane (MTES) in various proportions. Infusions of the precursors were performed in CO_2 at 60 °C and 123 bar (1 bar = 10^5 Pa) and the templates were removed by calcination in air at 400 °C for 6 h. Figures 1a,b show the XRD patterns for the as-infused and calcined films, respectively. As the MTES/TEOS ratio increased from 0:100 to 50:50, the *d*-spacing of the primary Bragg peak decreased from 71.2 to 54 Å for the as-infused films (traces 1,5 in Fig. 1).[21] In addition, the decrease in the intensity of the Bragg peak suggests a loss in the long-range order in organosilicate films. This is also evident in the XRD pattern of the 75:25 MTES/TEOS as-infused organosilicate film, which shows only a weak shoulder peak (trace 7 in Fig. 1). Upon calcination of the films, the Bragg peaks shifted to lower *d*-spacings due to uniaxial shrinkage perpendicular to the substrate. Except for the 75:25 organosilicate film, all the mesoporous films exhibit a high degree of order. The primary Bragg peak *d*-spacings for the as-infused and the calcined films are given in Table 1. The morphologies of the films were also investigated using TEM (see Fig. 2). Figures 2a,b show the cubic mesostructure of the Brij-78-templated mesoporous silica film along the [100] and [110] orientations. The peaks in the XRD patterns for the as-infused and calcined silica films are consis-

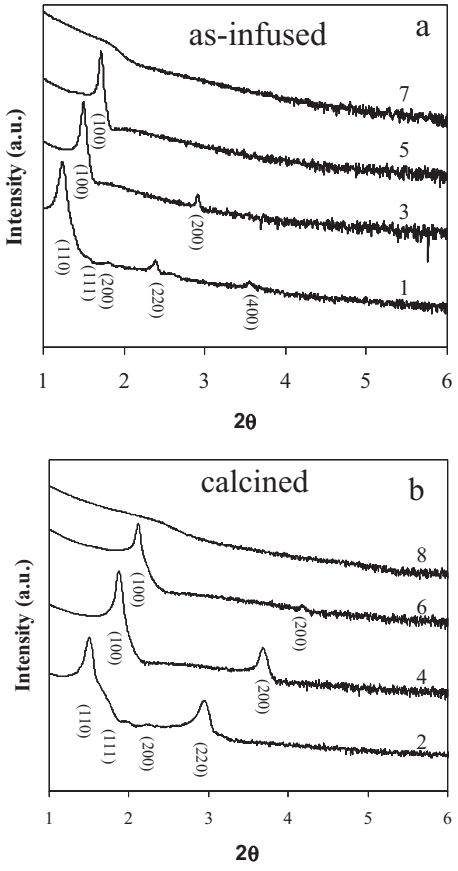

Figure 1. Conventional θ–θ XRD patterns for the a) as-infused and b) calcined mesostructured silicate and organosilicate films that were templated using Brij 78. All films were synthesized in CO_2 at 60 °C and 123 bar (1 bar = 10^5 Pa) using mixtures of TEOS and MTES in various proportions. Calcination was performed at 400 °C for 6 h in air. Traces 1,2 are for pure TEOS, traces 3,4 are for a 25:75 MTES/TEOS precursor mixture, traces 5,6 are for a 50:50 MTES/TEOS mixture, and traces 7,8 are for a 75:25 MTES/TEOS mixture. The *d*-spacings of the peaks and the morphologies of the films are described in Table 1.

Table 1. Properties of mesoporous silica and organosilicate films using Brij 78 as structure directing agent.

Precursor amounts		*d*-Spacing of primary peak [Å]		Morphology	Refractive index (*n*)
MTES	TEOS	As-infused	Calcined		
0	100	71.2 [a]	58.7 [b]	cubic	1.38
25	75	58.9 [c]	47.1 [d]	2D hexagonal	1.35
50	50	54 [e]	41.7 [f]	2D hexagonal disordered	1.31
75	25	–	–	disordered	1.25

[a] Strong Bragg peaks were observed at 71.2, 57.8, 49.9, and 36.8 Å, consistent with the (110), (111), (200), and (220) reflections of a cubic mesostructure, respectively. [b] Sharp Bragg peaks were observed at 58.7, 46.1, and 29.9 Å, consistent with the (110), (111), and (220) reflections, respectively, of a cubic morphology. [c] Strong Bragg peaks attributed to the (100) and (200) reflections of a two-dimensional (2D) hexagonal mesostructure were observed at 58.9 and 30.1 Å. A weak peak observed at 35.1 Å was consistent with the (110) reflection. [d] Possible (100) and (200) reflections for a 2D hexagonal mesostructure were observed at 47.1 and 24 Å, respectively. [e] No higher-order peaks observed. [f] The strong peak at 41.7 Å and a weak peak at 21.1 Å are consistent with the (100) and (200) reflections, respectively, of a 2D hexagonal disordered mesostructure.

tent with cubic mesostructures, with unit-cell parameters of 101.3 and 82.6 Å, respectively. In the case of the 25:75 MTES/TEOS mesoporous film, a two-dimensional (2D) hexagonal mesostructure is evident from the TEM lattice images that show the hexagonal arrangement of the cylindrical pores (see Fig. 2c) and a side view of the cylindrical channels (see Fig. 2d) along with the corresponding electron-diffraction patterns. The corresponding XRD patterns are consistent with 2D hexagonal mesostructures with unit-cell parameters of 68.5 and 55 Å for the as-infused and the calcined films, respectively. The 50:50 MTES/TEOS mesoporous film has a 2D disordered morphology, as is evident in the TEM images and the electron-diffraction patterns (see Figs. 2e,f). TEM studies showed that the 75:25 MTES/TEOS mesoporous film was completely disordered, as indicated by the absence of strong Bragg peaks in the XRD pattern. Thus, increased amounts of MTES in the precursor mixture resulted in a transition from a cubic-packed spherical to a 2D hexagonal cylindrical to a disordered morphology. The final morphology is coupled to the nature of the precursor, which affects the hydrophilic–hydrophobic balance of the structure-directing agent[22] and the degree of infusion.[14,23]

The presence of pendant methyl groups derived from the MTES precursor in the framework of the calcined mesoporous films increases the hydrophobicity of the films. For the film prepared using TEOS only, the presence of hydroxyl vibrations (isolated Si–OH at 3743 cm^{-1} and a broad conjugated OH absorbance at 3521 cm^{-1}) in FTIR spectra indicate a hydrophilic framework (Fig. 3b).[24,25] As MTES is incorporated into the films, a decrease of the hydroxyl absorbance accompanied by an increase in the CH vibrations (2980 and 2928 cm^{-1}) of the pendant methyl groups was observed.[3] The Si–O–Si antisymmetric stretching absorbance peak shifted to low frequencies, from 1080 to 1044 cm^{-1}, as the MTES/TEOS

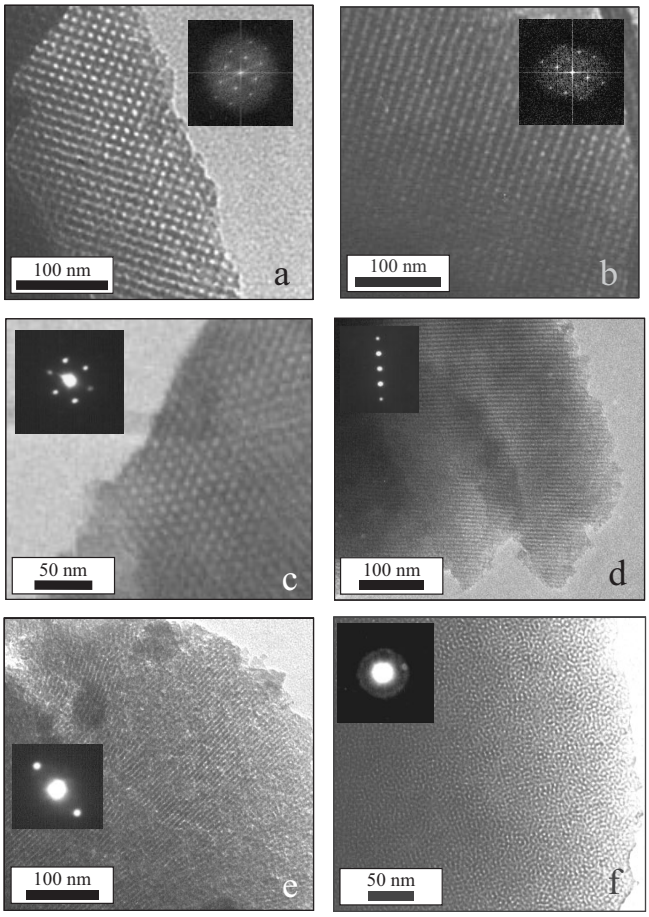

Figure 2. TEM images recorded for a mesoporous silica film using Brij 78 as the template, along the a) [100] and b) [110] orientations of a cubic mesostructure. The insets of the images show the corresponding Fourier diffractograms. c,d) TEM images and electron-diffraction patterns (insets) of a two-dimensional (2D) hexagonal mesostructure of a Brij-78-templated mesoporous organosilicate film. The film was synthesized using a 25:75 mixture of MTES/TEOS. e,f) TEM images and electron-diffraction patterns (insets) of a 2D hexagonal mesostructure with a disordered wormhole morphology. The wormhole morphology is shown in (f), while in (e) a more ordered cylindrical region of the organosilicate film is shown.

ratio increased from 0:100 to 75:25 (Fig. 3a).[26] The absorbance bands of the pendant methyl groups at 784, 1278, and 1422 cm^{-1} also increased,[24] indicating that the methyl groups survived the calcination step. Rutherford backscattering (RBS) studies on similar calcined mesoporous organosilicate films showed a uniform composition over the entire thickness that depended on the molar composition of the organosilicate precursors.[27] The increase in the hydrophobicity of the films is also evident from the refractive indices of the calcined mesoporous films (Table 1). The refractive index decreased from 1.38 for the TEOS film to 1.31 for the 50:50 MTES/TEOS film[5] as a result of decreased adsorption of water on the hydrophobic pore surface.

Mesoporous organosilicate films were also prepared using bridged silsesquioxanes ($(RO)_3Si–R'–Si(OR)_3$) as precursors,

ADVANCED MATERIALS

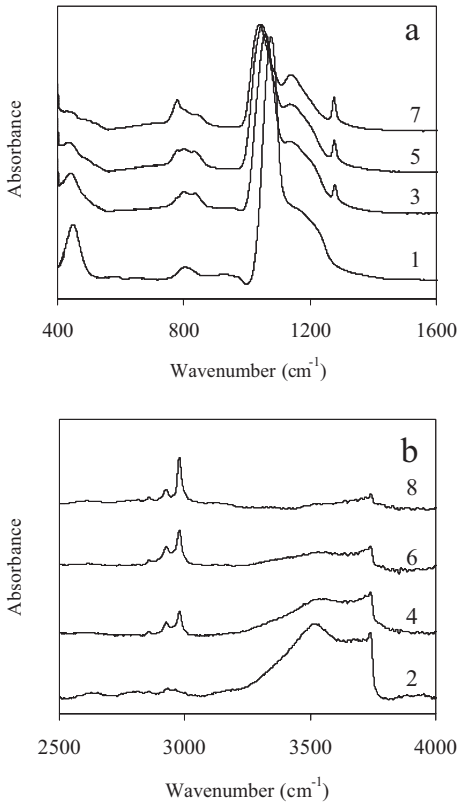

Figure 3. FTIR spectra of mesoporous silica and organosilicate films in the a) 400 to 1600 cm^{-1} and b) 2500 to 4000 cm^{-1} ranges. The films were prepared using pure TEOS (traces 1,2), 25:75 MTES/TEOS (traces 3,4), 50:50 MTES/TEOS (traces 5,6), and 75:25 MTES/TEOS (traces 7,8).

to yield a uniform distribution of the organic group R′ in the framework.[11] The bridging group can be alkanes, alkenes or aromatic groups. Figure 4 shows a TEM image of a mesostructured organosilicate film that was prepared using bis(triethoxysilyl)ethane as the precursor and Pluronic F108 ($PEO_{133}PPO_{50}PEO_{133}$) as the organic template. The presence of the organic groups in the calcined mesoporous film was confirmed using FTIR spectroscopy, which showed absorbance bands at 1270, 1430, 2980, and 2930 cm^{-1} because of the presence of the bridging methylene groups in the framework.[24] We have also prepared mesoporous materials using other bridged precursors, including bis(triethoxysilyl)methane and bis(triethoxysilyl)ethylene. The alkene groups provide a reactive handle within the backbone for subsequent functionalization.

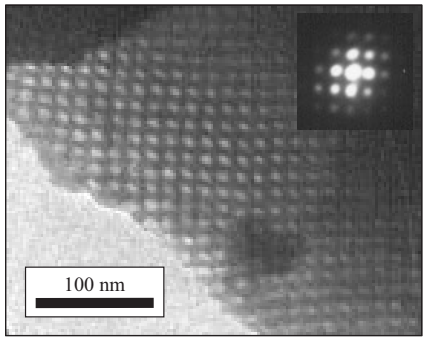

Figure 4. TEM image and electron-diffraction pattern (inset) of a calcined mesostructured organosilicate film that was prepared using bis(triethoxysilyl)ethane, $(EtO)_3Si–C_2H_4–Si(OEt)_3$, as the inorganic precursor and Pluronic F108 as the structure-directing agent.

Finally, we have functionalized mesoporous silica films prepared in CO_2 by subsequent surface modification in CO_2.[12] Figure 5a shows FTIR difference spectra associated with the capping of pore-surface silanols in a calcined mesoporous silica film by exposure to hexamethyldisilazane (HMDS) in a supercritical CO_2 solution at 50 °C and 90 bar for one minute. The cubic mesoporous silica film was synthesized using TEOS and Pluronic F108.[14] The spectrum of the unmodified silica film was subtracted from that of the modified film. The FTIR difference spectrum shows a decrease in the OH-absorption peaks at 980 and 3746 cm^{-1}, an increase in the Si–CH_3-absorption peaks at 1260 and 759 cm^{-1}, Si–O–Si-peaks at 450, 850, and 1000–1250 cm^{-1}, and the CH-stretching absorption peaks at 2964 and 2908 cm^{-1}.[19] The FTIR difference spectra for the capping of the surface silanols with other silane coupling agents, such as *n*-octyl trichlorosilane (OTCS) and *N*-methyl aminopropyltrimethoxysilane (NMAPTMS) in supercritical CO_2 at 60 °C and 204 bar for 30 min and 1 h, respectively, are shown in Figures 5b,c, respectively. The OTCS post-treatment was followed by a thermal treatment at 200 °C for 1 h in air. The absence of physisorbed OTCS is indicated by the absence of the characteristic Si–Cl peaks at 590 and 568 cm^{-1}, and the shifted peak at 3697 cm^{-1} for isolated Si–OH groups.[19] The characteristic Si–O–Si stretching peaks at 1000–1250 and 813 cm^{-1}, and other characteristic CH peaks at 1422, 1466, and 2800–3000 cm^{-1}, indicate the presence of hydrolyzed OTCS.[19] In the case of NMAPTMS functional-

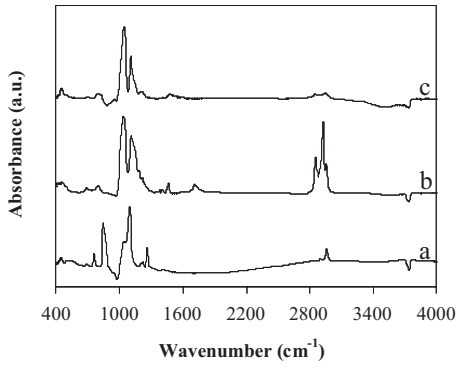

Figure 5. a) FTIR difference spectrum for the HMDS treatment of a mesoporous silica film in CO_2 at 50 °C and 90 bar for 1 min. The reference spectrum of the unmodified silica film was subtracted directly from the spectrum of the modified film. FTIR difference spectra for b) *n*-octyltrichlorosilane (OTCS) and c) *N*-methylpropyltrimethoxysilane (NMAPTMS) treatment in CO_2 at 60 °C and 204 bar.

ization, the weak CH-stretching peak at ~2708 cm^{-1} corresponds to the N–CH_3 peak and indicates the effectiveness of the coupling chemistry.[24]

Experimental

Synthesis and Characterization: For the direct co-condensation synthesis, films of the organic templates were spin-coated from a ~5 % solution of the template and *p*TSA in ethanol on cleaned high-resistivity silicon wafers. The ratio of the weight of *p*TSA to the template in the solution was maintained at 0.06. The template films were then exposed to a solution of the inorganic oxide precursors in humidified supercritical CO_2 in a high-pressure reactor. The total precursor amount varied from 4.5 to 5 μg for a template film cast on a 1.75 in. × 1.75 in. square piece of silicon wafer All film syntheses were performed in CO_2 at 60 °C and 123 bar for 2 h. The reactor was then slowly depressurized. Removal of the organic template by calcination at 400 °C in air for 6 h yielded a porous organosilicate film. For the post-synthesis functionalization, the calcined silica film was exposed to the solution of the silane-coupling agent in dry supercritical CO_2. After a brief reaction time, the reactor was depressurized within a couple of minutes.

XRD patterns were obtained using Cu Kα radiation (wavelength, $\lambda = 1.5418$ Å) using a Philips X'Pert PW3040-MPD diffractometer operating at 45 kV and 40 mA in the conventional θ–θ Bragg–Brentano diffraction geometry. FTIR spectra of the films were obtained on silicon wafers in a BioRad ExCalibur spectrometer in the transmission mode with a resolution of 4 cm^{-1}, using the blank wafers as the reference spectrum, by the co-addition of 200 scans. TEM images were obtained using JEOL 100 CX and JEOL 2000 FX microscopes that were operated at 100 and 200 kV, respectively. The samples were prepared by scraping off the films to prepare a slurry of the particles in ethanol. Drops of the slurry were dropped on a formvar-coated copper grid (Electron Microscopy Sciences) and dried prior to use. SE measurements were performed on a Sopra GES5 variable-angle spectroscopic ellipsometer. The incident angle for all measurements was fixed at 75° from the vertical and the wavelength was varied from 250 to 900 nm. A four-layer model comprised of air, silica dielectric layer of unknown thickness and refractive index, native Si oxide, and silicon crystal layer, was used to fit the data. The fitting parameters were the thickness and the refractive index of the silica dielectric layer.

Received: November 24, 2004
Final version: October 17, 2005
Published online: December 21, 2005

[1] J. Y. Ying, C. P. Mehnert, M. S. Wong, *Angew. Chem. Int. Ed.* **1999**, *38*, 56.
[2] G. Wirnsberger, B. J. Scott, G. D. Stucky, *Chem. Commun.* **2001**, 119.
[3] F. K. de Theije, A. R. Balkenende, M. A. Verheijen, M. R. Baklanov, K. P. Mogilnikov, Y. Furukawa, *J. Phys. Chem. B* **2003**, *107*, 4280.
[4] a) G. Xomeritakis, C. M. Braunbarth, B. Smarsly, N. Liu, R. Kohn, Z. Klipowicz, C. J. Brinker, *Microporous Mesoporous Mater.* **2003**, *66*, 91. b) Z. P. Lai, G. Bonilla, I. Diaz, J. G. Nery, K. Sujaoti, M. A. Amat, E. Kokkoli, O. Terasaki, R. W. Thompson, M. Tsapatsis, D. G. Vlachos, *Science* **2003**, *300*, 456.
[5] A. R. Balkenende, F. K. de Theije, J. C. K. Kriege, *Adv. Mater.* **2003**, *15*, 139.
[6] a) Y. Lu, R. Ganguli, C. A. Drewien, M. T. Anderson, C. J. Brinker, W. Gong, Y. Guo, H. Soyez, B. Dunn, M. H. Huang, J. I. Zink, *Nature* **1997**, *389*, 364. b) D. Zhao, P. Yang, N. A. Melosh, J. Feng, B. F. Chmelka, G. D. Stucky, *Adv. Mater.* **1998**, *10*, 1380.
[7] a) H. Yang, N. Coombs, I. Sokolov, G. A. Ozin, *Nature* **1996**, *381*, 589. b) H. Yang, A. Kuperman, N. Coombs, S. Mamiche Afara, G. A. Ozin, *Nature* **1996**, *379*, 703. c) H. W. Hillhouse, T. Okubo, J. W. V. Egmond, M. Tsapatsis, *Chem. Mater.* **1997**, *9*, 1505. d) I. A. Aksay, M. Trau, S. Manne, I. Honma, N. Yao, L. Zhou, P. Fenter, P. M. Eisenberger, S. M. Gruner, *Science* **1996**, *273*, 892.
[8] X. Feng, G. E. Fryxell, L.-Q. Wang, A. Y. Kim, J. Liu, K. M. Kemner, *Science* **1997**, *276*, 923.
[9] M. H. Lim, A. Stein, *Chem. Mater.* **1999**, *11*, 3285.
[10] a) S. Guan, S. Inagaki, T. Ohsuna, O. Terasaki, *J. Am. Chem. Soc.* **2000**, *122*, 5660. b) S. Inagaki, S. Guan, Y. Fukushima, T. Ohsuna, O. Terasaki, *J. Am. Chem. Soc.* **1999**, *121*, 9611. c) T. Asefa, M. J. MacLachlan, N. Coombs, G. A. Ozin, *Nature* **1999**, *402*, 867. d) T. Asefa, M. J. MacLachlan, H. Grondey, N. Coombs, G. A. Ozin, *Angew. Chem. Int. Ed.* **1999**, *39*, 1808. e) K. Yu, B. Smarsly, C. J. Brinker, *Adv. Funct. Mater.* **2003**, *13*, 47. f) K. Yu, X. Wu, C. J. Brinker, J. Ripmeester, *Langmuir* **2003**, *19*, 7282.
[11] Y. Lu, H. Fan, N. Doke, D. A. Loy, R. A. Assink, D. A. LaVan, C. J. Brinker, *J. Am. Chem. Soc.* **2000**, *122*, 5258.
[12] A. Sayari, S. Hamoudi, *Chem. Mater.* **2001**, *13*, 3151.
[13] B. Xie, A. J. Muscat, presented at the *8th Int. Symp. on Cleaning Technology in Semiconductor Devices*, Orlando, FL 2003.
[14] R. A. Pai, R. Humayun, A. Sengupta, J.-N. Sun, M. T. Schulberg, J. J. Watkins, *Science* **2004**, *303*, 507.
[15] R. R. Gupta, V. S. RamachandraRao, J. J. Watkins, *Macromolecules* **2003**, *36*, 1295.
[16] B. D. Vogt, G. D. Brown, V. S. RamachandraRao, J. J. Watkins, *Macromolecules* **1999**, *32*, 7907.
[17] P. D. Condo, S. R. Sumpter, M. L. Lee, K. P. Johnston, *Ind. Eng. Chem. Res.* **1996**, *35*, 1115.
[18] a) C. T. Cao, A. Y. Fadeev, T. J. McCarthy, *Langmuir* **2001**, *17*, 757. b) X. Q. Jia, T. J. McCarthy, *Langmuir* **2002**, *18*, 683. c) C. P. Tripp, J. R. Combes, *Langmuir* **1998**, *14*, 7350.
[19] J. R. Combes, L. D. White, C. P. Tripp, *Langmuir* **1999**, *15*, 7870.
[20] D. L. Goldfarb, J. J. de Pablo, P. F. Nealey, J. P. Simons, W. M. Moreau, M. Angelopoulos, *J. Vac. Sci. Technol., B* **2000**, *18*, 3313.
[21] M. Kruk, T. Asefa, N. Coombs, M. Jaroniec, G. A. Ozin, *J. Mater. Chem.* **2002**, *12*, 3452.
[22] J. M. Kim, Y. Sakamoto, Y. K. Hwang, Y.-U. Kwon, O. Terasaki, S. E. Park, G. D. Stucky, *J. Phys. Chem. B* **2002**, *106*, 2552.
[23] P. Alberius, K. L. Frindell, R. C. Hayward, E. J. Kramer, G. D. Stucky, B. F. Chmelka, *Chem. Mater.* **2002**, *14*, 3284.
[24] N. B. Colthup, L. H. Daly, S. E. Wiberley, *Introduction to Infrared and Raman Spectroscopy*, Academic Press, Inc., San Diego, CA **1990**.
[25] P. Innocenzi, *J. Non-Cryst. Solids* **2003**, *316*, 309.
[26] T. Nakano, T. Tokunaga, T. Ohta, *J. Electrochem. Soc.* **1995**, *142*, 1303.
[27] B. D. Vogt, R. A. Pai, H.-J. Lee, R. C. Hedden, C. L. Soles, W.-L. Wu, E. K. Lin, B. J. Bauer, J. J. Watkins, *Chem. Mater.* **2005**, *17*, 1398.

